Developmental Cell
Article

A Molecular Network for the Transport of the TI-VAMP/VAMP7 Vesicles from Cell Center to Periphery

Andrea Burgo,[1,2,*] Véronique Proux-Gillardeaux,[1,2] Emmanuel Sotirakis,[1,2] Philippe Bun,[1] Alessandra Casano,[1,2] Agathe Verraes,[1,2] Ronald K.H. Liem,[3] Etienne Formstecher,[4] Maïté Coppey-Moisan,[1] and Thierry Galli[1,2,*]
[1]Institut Jacques Monod, UMR 7592, CNRS, Université Paris Diderot, Sorbonne Paris Cité, F-75205 Paris, France
[2]INSERM ERL U950, Membrane Traffic in Neuronal and Epithelial Morphogenesis, F-75013 Paris, France
[3]Department of Pathology and Cell Biology, Taub Institute for Research on Alzheimer's Disease and Aging Brain, Columbia University College of Physicians and Surgeons, New York City, NY 10032, USA
[4]Hybrigenics, F-75014 Paris, France
*Correspondence: burgo.andrea@ijm.univ-paris-diderot.fr (A.B.), thierry.galli@inserm.fr (T.G.)
DOI 10.1016/j.devcel.2012.04.019

SUMMARY

The compartmental organization of eukaryotic cells is maintained dynamically by vesicular trafficking. SNARE proteins play a crucial role in intracellular membrane fusion and need to be targeted to their proper donor or acceptor membrane. The molecular mechanisms that allow for the secretory vesicles carrying the v-SNARE TI-VAMP/VAMP7 to leave the cell center, load onto microtubules, and reach the periphery to mediate exocytosis are largely unknown. Here, we show that the TI-VAMP/VAMP7 partner Varp, a Rab21 guanine nucleotide exchange factor, interacts with GolginA4 and the kinesin 1 Kif5A. Activated Rab21-GTP in turn binds to MACF1, an actin and microtubule regulator, which is itself a partner of GolginA4. These components are required for directed movement of TI-VAMP/VAMP7 vesicles from the cell center to the cell periphery. The molecular mechanisms uncovered here suggest an integrated view of the transport of vesicles carrying a specific v-SNARE toward the cell surface.

INTRODUCTION

Intracellular vesicular traffic in eukaryotes relies on three major steps: the formation of a vesicular or tubular intermediate from a donor membrane, the transport of this intermediate along cytoskeletal elements (actin and/or microtubules), and finally the docking and fusion with the acceptor membrane. Secretory vesicles (SVs) are formed at the trans-Golgi network (TGN), located close to the microtubule organizing center (MTOC) in the cell center, and then are transported to the cell periphery, where they fuse with the plasma membrane (PM) (Pfeffer, 2007). Reaching the cell periphery is an important issue for SVs in all cells but is a particularly challenging problem in neurons, where they must often travel great distances along neurites to participate in the formation and growth of membrane protrusions (Pfenninger, 2009). Newly synthesized SVs are transported along microtubules (MTs) from the TGN to the PM by specific molecular motors. Because of the polarity of MTs (minus-ends in the center, plus-ends in the periphery), center to periphery motors are kinesins in most cases (Hoogenraad and Bradke, 2009; Verhey et al., 2011). How a nascent SV is put on the track to be transferred from the cell center to the cell periphery is largely unknown.

After transport of the vesicle to its destination, SNAREs mediate the final step of membrane fusion. Vesicular (v-) and target (t-) SNAREs form a so-called trans-SNARE complex, which is required to merge the two membranes. SNAREs function as fusion proteins only when the distance between donor and acceptor membranes becomes less than 10 nm (Li et al., 2007), and therefore upstream targeting and tethering mechanisms are crucial to properly position the vesicle such that the v- and t-SNAREs can operate productively. The v-SNARE TI-VAMP/VAMP7 (TI-VAMP) was previously shown to mediate the exocytosis of SVs and granules of different types (Chaineau et al., 2008), including those containing VSV-G in HeLa cells (Danglot et al., 2010). TI-VAMP-mediated exocytosis is particularly active in early phases of axon formation (Gupton and Gertler, 2010) and Netrin-1-dependent attraction (Cotrufo et al., 2011) in cultured neurons. It may later be involved in neurotransmitter release (Hua et al., 2011; Scheuber et al., 2006) and higher brain function (Danglot et al., 2012). Interactions of SNAREs with molecular coats have been shown previously to be important for targeting. For instance, direct interaction of TI-VAMP with AP-3 and Hrb allows for its sorting and recycling, respectively (Chaineau et al., 2008; Martinez-Arca et al., 2003; Pryor et al., 2008; Scheuber et al., 2006). In addition, SNARE function and SV traffic are regulated by Rab GTPases (Grosshans et al., 2006; Stenmark, 2009). Interestingly, TI-VAMP interacts with Varp (Burgo et al., 2009; Tamura et al., 2011), a GEF for Rab21 (Zhang et al., 2006). However, how TI-VAMP vesicles are addressed to the cell periphery is still largely unknown. Here, we demonstrate that TI-VAMP exocytosis occurs at distal neurites in living neurons and that TI-VAMP vesicles move on MTs. We found that Varp interacts with the molecular motor kinesin 1 Kif5A, which regulates the transport of TI-VAMP to growth cones. We further show that

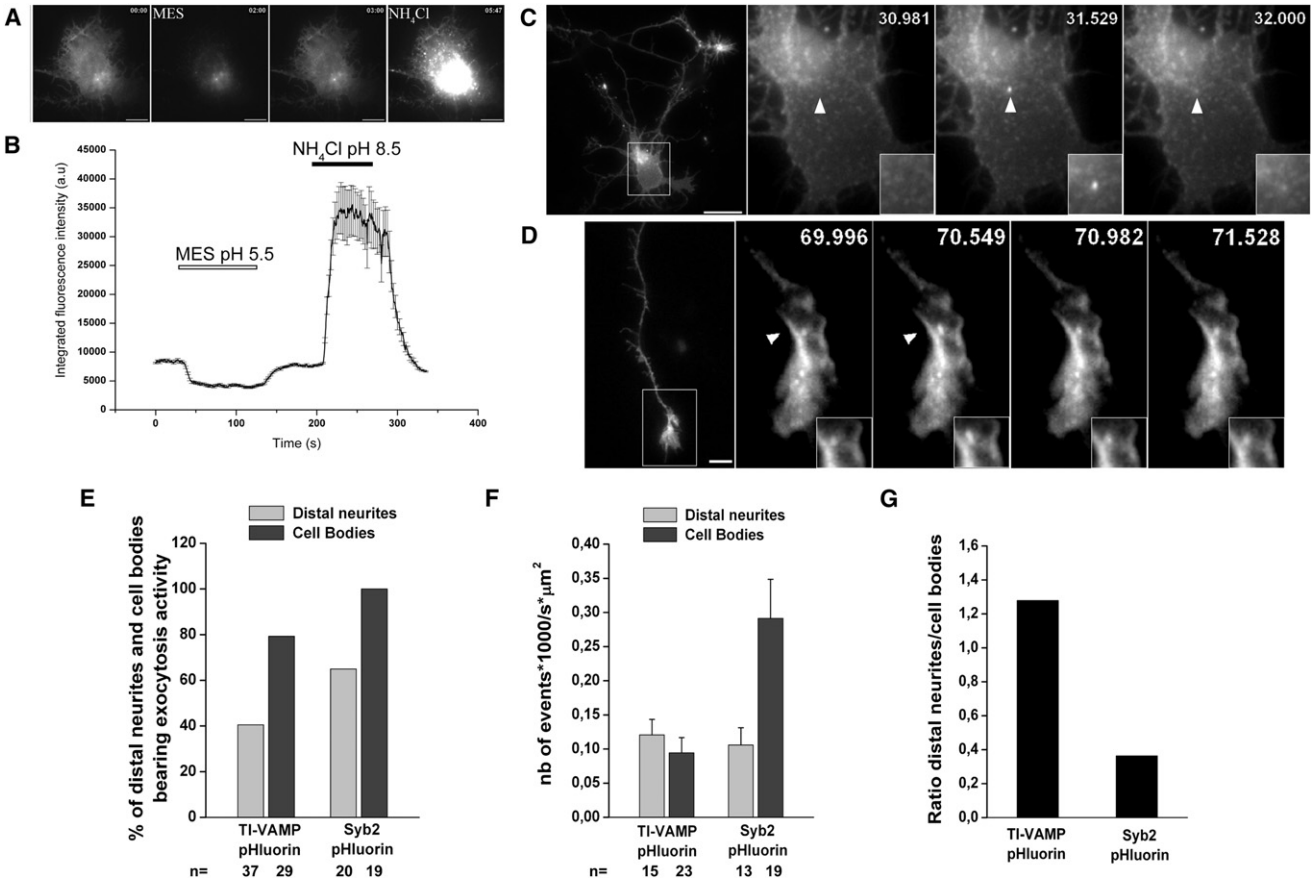

Figure 1. TI-VAMP Exocytosis Occurs at the Growth Cone

(A and B) Effect of pH on TI-VAMP-pHluorin fluorescence intensity in rat hippocampal neurons at 3-DIV. (A) Cultured rat hippocampal neurons were transfected with TI-VAMP-pHluorin at 2-DIV and imaged live at 3-DIV. Snapshots show the effect of acidification (MES pH 5.5) and alkalization (NH_4Cl 50 mM) on TI-VAMP-pHluorin fluorescence intensity. Time is indicated in min:sec. Scale bar, 10 µm. (B) The change in average fluorescence intensity is plotted as a function of time.

(C and D) Transient exocytic events of TI-VAMP-pHluorin (arrowheads and insets) in cell body (C, scale bar, 20 µm) and distal neurite (D, scale bar, 5 µm) of rat hippocampal neuron at 3-DIV. Time is indicated in sec:msec.

(E) Percentage of distal neurites and cell bodies bearing TI-VAMP- or Syb2- pHluorin exocytic activity in rat hippocampal neurons at 3-DIV.

(F) Quantification of the density × 1,000 per second of exocytic events for TI-VAMP- or Syb2- pHluorin, both in distal neurites and cell bodies. Data are shown as mean ± SEM.

(G) Ratio between the density × 1,000 per second of exocytic events at the distal neurites and cell bodies, both of TI-VAMP- and Syb2- pHluorins. n = numbers of distal neurites or cell bodies analyzed.

See also Figure S1 and Movies S1 and S2.

Rab21 regulates the transport of TI-VAMP vesicles and their exocytosis. Moreover, Varp interacts with GolginA4/p230 and Rab21, in its GTP bound state, with microtubule and actin cross-linking factor 1 (MACF1), an actin and microtubule regulator and a partner of GolginA4 (Kakinuma et al., 2004). Both MACF1 and GolginA4 regulate transport of TI-VAMP from cell center to periphery. We thus suggest that TI-VAMP recruits a dynamic molecular network to coordinate molecular mechanisms allowing for SV transport to the cell periphery.

RESULTS

TI-VAMP Is Exocytosed at the Distal Portion of Neurites and Is Transported along MTs

TI-VAMP accumulates in neuronal growth cones (Alberts et al., 2003; Coco et al., 1999) and mediates an important secretory pathway in neurons cultured in vitro (Cotrufo et al., 2011; Gupton and Gertler, 2010; Hua et al., 2011). To assess the distribution and the rate of TI-VAMP exocytosis in neurons, we monitored the exocytic events of TI-VAMP fused to the superecliptic pHluorin (Sankaranarayanan et al., 2000) by fast time-lapse video imaging as recently used in developing neurons (Gupton and Gertler, 2010). At the same time we analyzed the exocytosis of Syb2-pHluorin, a major v-SNARE of mature synaptic vesicles, which is also transported to growth cones in immature neurons (Tojima et al., 2007). Rat hippocampal neurons were transfected after 2 days of culture in vitro (2-DIV) with TI-VAMP- or Syb2-pHluorin and analyzed at 3-DIV, a stage of active axonal growth. Acidification with the weakly acidic MES buffer and alkalinization with the cell-permeant weak base NH_4Cl (50 mM) confirmed the expression of TI-VAMP-pHluorin within an acidic, intracellular compartment in developing neurons (Figures 1A and 1B),

as previously shown in more mature neurons (Hua et al., 2011). Both TI-VAMP- and Syb2- pHluorins showed transient exocytic events at resting condition in the cell body (Figure 1C; Figure S1A and Movies S1 and S2 available online) and at the distal part of the longest neurites, i.e., axons, which we herein defined as "distal neurites" (Figures 1D and S1B; Movies S1 and S2). Field electrical stimulation and KCl-induced depolarization did not increase the frequency of TI-VAMP exocytosis in our experimental conditions (data not shown), suggesting that TI-VAMP vesicles exocytosed spontaneously in developing neurons. Quantification of the numbers of exocytic events normalized for the analyzed surface area and time revealed that Syb2 exocytosed more frequently in cell bodies than in distal neurites, whereas TI-VAMP exocytosis events did not differ significantly in these two regions (Figures 1E and 1F). The ratio between exocytosis at distal neurites and within cell bodies, both for TI-VAMP- and Syb2- pHluorins, showed that the balance of exocytic events is shifted to the distal neurite for TI-VAMP compared to Syb2 (Figure 1G). These data suggest the occurrence of a particularly active transport of TI-VAMP-containing vesicles to distal neurites.

We have recently shown that TI-VAMP vesicles are in close proximity to the MT network in HeLa cells (Burgo et al., 2009), suggesting that they move along MTs despite earlier studies suggesting a more static behavior (Advani et al., 1999). Here we studied the dynamics of mRFP-TI-VAMP by time-lapse video imaging in hippocampal neurons in culture coexpressing GFP-Tubulin to visualize MTs. We found that long-range bidirectional movements of TI-VAMP occurred along MT tracks (Figure 2A and Movie S3). To further confirm that TI-VAMP vesicles moved on the MT network, we destabilized MTs by 1 μM nocodazole treatment and monitored the dynamics of GFP-TI-VAMP vesicles (Figure 2B and Movie S4). Coexpression of Cherry-TAU confirmed the depolymerization effect of nocodazole. The dynamics of GFP-TI-VAMP vesicles was measured by spatial temporal image correlation spectroscopy (STICS) (Hebert et al., 2005; Wiseman et al., 2004) (Figure 2C and see Experimental Procedures). Fifteen minutes after nocodazole treatment, when MT depolymerization was evident (as monitored by loss of Cherry-TAU fluorescence, Figure 2B), the motility of TI-VAMP vesicles was drastically reduced (Figure 2D). These results suggest that TI-VAMP vesicles interact with and move along MTs.

Varp Interaction with Kif5A Targets TI-VAMP to Growth Cones

The colocalization of TI-VAMP and Varp on MTs (Burgo et al., 2009) led us to search for partners of Varp that could potentially interact with MTs. In a yeast two-hybrid screen (Y2HS) using a fetal brain library and the full-length Varp as bait, we identified the neuronal molecular motor kinesin Kif5A as an interacting partner (Figure 3A). The interaction domain (ID), identified by Y2HS, lies within the C-terminal portion, a region conserved in the Kif5 subfamily (Figure S2A) and previously found to interact with Kv3.1 voltage-gated K^+ channels to mediate their transport to axons (Xu et al., 2010). Immunoprecipitation using an antibody directed against Kif5A/B/C pulled down endogenous Varp from NGF-differentiated PC12 cells extract (Figure 3B), thus validating the interaction in vivo. Using full-length tagged Kif5A, and Kif5C, and GFP-tagged or untagged Varp, we showed that both Kif5A (Figure 3C, left) and Kif5C (Figure S2B) coimmunoprecipitated Varp. Coprecipitation of Varp with the GFP-tagged-interacting domain of Kif5A (GFP-Kif5A-ID) further confirmed that Kif5A-ID indeed corresponds to the bona fide interaction domain (Figure 3D, left). We tested the capacity of Kif5A-ID to act as a dominant negative, as previously demonstrated for the Kif5C C-terminal domain, through competition for partners of endogenous Kif5 heavy chain (Konishi and Setou, 2009). Kif5A-ID was overexpressed in rat hippocampal neurons at 3-DIV, and its effects on axonal length and the distribution of endogenous TI-VAMP were measured. As control, we analyzed neurons transfected with GFP alone or with GFP-Kif5A. Interestingly, we observed that Kif5A-ID concentrated in dendrites and was excluded from axons (Figures 3E and S2C). Because the intensity of fluorescence of the GFP-Kif5A-ID construct was weak along the axon (albeit detectable), for quantifications we coexpressed RFP to visualize axons (Figure 3E). Quantification of the axonal length showed that overexpression of Kif5A-ID impaired axonal growth compared with GFP and GFP-Kif5A (Figure 3F). Moreover, overexpression of Kif5A-ID inhibited the localization of endogenous TI-VAMP in growth cones (Figures 3G and 3H). We attempted to show that Kif5A-ID disrupts the Varp/Kif5A interaction but cotransfection of all three constructs produced inconsistent levels of expression. Instead, to further confirm the role of Kif5A in the transport of TI-VAMP to growth cones, we silenced the expression of Kif5A (Table 1) in young hippocampal neurons and found striking reduction of TI-VAMP staining in growth cones (Figures S2D–S2G). Taken together, these results demonstrate that the Kif5A tail interacts with Varp and that Kif5A is crucial to target TI-VAMP vesicles to growth cones, i.e., from cell center to periphery. The tail domain of Kif5C, previously used to inhibit axonal transport (Konishi and Setou, 2009), has a high level of sequence identity to Kif5A-ID (Figure S2A). Therefore, expression of either one of these dominant negative fragments is expected to have an effect on all Kif5 cargoes. Given the high level of sequence similarity, it is likely that Varp can interact with any of the Kif5 isoforms to mediate transport of TI-VAMP to the cell periphery.

Rab21 Regulates TI-VAMP Transport and Exocytosis

Varp is a guanine nucleotide exchange factor (GEF) for the small GTPase Rab21 (Zhang et al., 2006). Several Rabs have been shown to regulate vesicle motility along the cytoskeleton (Echard et al., 1998; Fukuda and Kuroda, 2002; Zerial and McBride, 2001). We previously found that Rab21 partially colocalizes with TI-VAMP vesicles and regulates neurite growth in PC12 cells (Burgo et al., 2009). Here we showed that both proteins were cotransported (Movie S5), suggesting a role of this small GTPase in TI-VAMP vesicle motility. To test this hypothesis, the directionality (anterograde versus retrograde) of TI-VAMP vesicles along growing neurites of differentiating PC12 cells expressing Rab21 in its wild-type (WT), dominant negative (T33N), or constitutively active (Q78L) forms was measured (Figure 4A and Movie S6). We found that a significant percentage of TI-VAMP vesicles moved preferentially in the anterograde direction in cells expressing Rab21-Q78L (Figure 4B), suggesting that active Rab21 promotes transport toward the cell periphery, whereas TI-VAMP vesicle directionality was not affected in cells

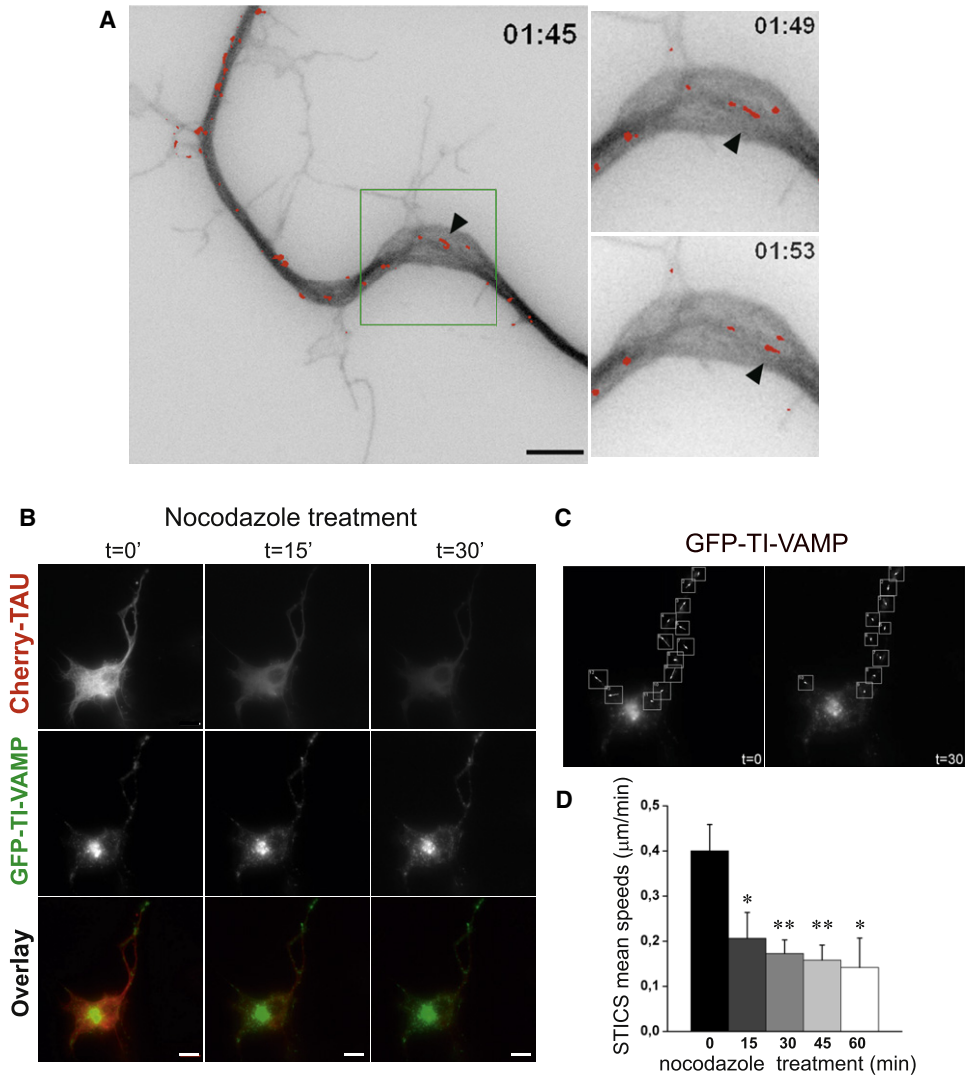

Figure 2. TI-VAMP Transport Depends on Microtubules

(A) Snapshots from Movie S3 showing binarized RFP-TI-VAMP (red) and GFP-Tubulin (black) in a rat hippocampal neurite. Arrowhead points to close apposition of RFP-TI-VAMP vesicles onto a GFP-tubulin track.

(B) Differentiated PC12 cells were cotransfected with GFP-TI-VAMP and a marker of MTs, Cherry-TAU. After 24 hr, the cells were treated with 1 μM nocodazole and imaged at 0, 15, and 30 min after treatment.

(C) STICS analysis was performed on selected regions of 32 × 32 or 64 × 64 pixels to reveal speed and directionality (white arrows in boxed areas) of TI-VAMP-containing vesicles in cells (see Experimental Procedures).

(D) Statistical analysis of RFP-TI-VAMP vesicle speeds before and after nocodazole treatment. Data are shown as mean ± SEM. Significance is determined by one-way ANOVA, Tukey's posttest. *$p < 0.05$, **$p < 0.01$. Time is indicated in min:sec. Scale bar, 10 μm.

See also Movies S3 and S4.

expressing Rab21-WT or Rab21-T33N. In addition, we found that the endogenous TI-VAMP was redistributed closer to the nucleus in GFP-Rab21-T33N cells and toward the cell periphery in GFP-Rab21-Q78L cells, whereas Syb2 distribution was not significantly modified in NGF-differentiated PC12 cells (Figures S3A–S3D). To determine whether the Rab21 mutants also affect the speed of TI-VAMP-containing vesicles, we measured both average (excluding motionless periods) and maximum speeds. The speed of an individual anterograde or retrograde vesicle ranged from ~0 μm/s (motionless vesicle) to ~2 μm/s in agreement with previous observations for other SVs (Hill et al., 2004; Lochner et al., 1998). Analysis of the anterograde and retrograde mean speeds (Figures 4C and 4D, left; Figures S3E and S3F) showed that the expression of Rab21-Q78L significantly decreased the anterograde speed compared to the Rab21-WT and Rab21-T33N-expressing cells. Similarly, Rab21-Q78L significantly decreased the anterograde speed compared to the Rab21-T33N in rat hippocampal neurons (Figures 4C and 4D, right). On the contrary, retrograde velocities were not significantly affected by Rab21 mutants. The paradoxical effect of Rab21-Q78L on TI-VAMP vesicle dynamics, in which more vesicles move in the anterograde direction but more slowly, could be

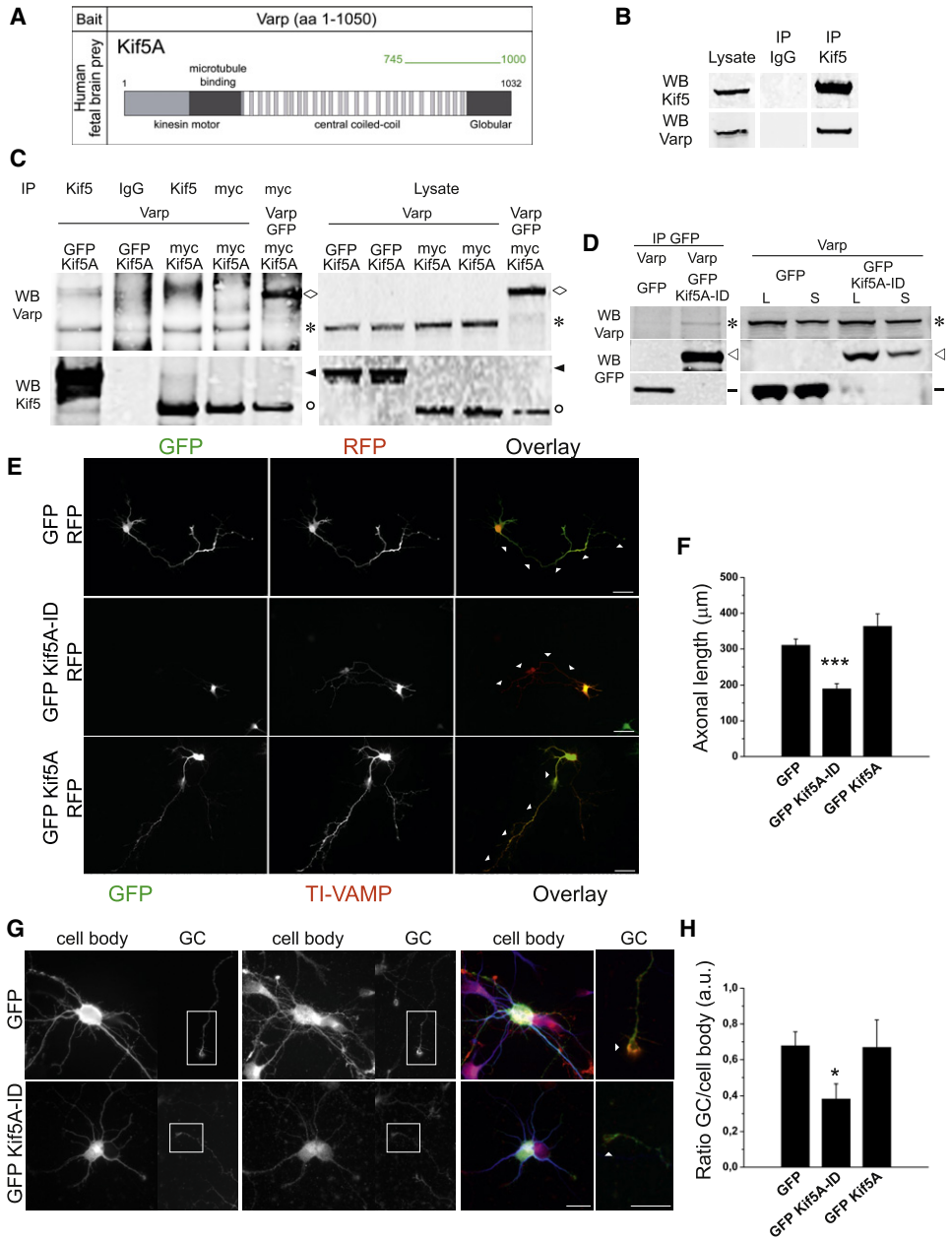

Figure 3. Kif5A, a Partner of Varp, Acts as a Molecular Motor for TI-VAMP Vesicles

(A) Kif5A was identified as a partner of Varp in an Y2HS using full-length Varp as bait and a human fetal brain cDNA library. Kif5A was found in only four other screens out of the 165 performed with different baits and the same human fetal brain library (data not shown). The fragment(s) identified in each screen were distinct (different start or stop positions). This strongly suggests that Kif5A is a bona fide interacting partner of Varp. The green line highlights the total coverage of all prey clones identified in the screens.

(B) Endogenous Varp coimmunoprecipitated with endogenous Kif5 in NGF-differentiated PC12 cells.

(C) Varp coprecipitates with full-length Kif5A. COS-7 cells were cotransfected with untagged Varp or Varp-GFP and GFP-Kif5A or Kif5A-myc. After 24 hr, proteins were extracted and immunoprepicipitation was performed using monoclonal antibody against Kif5 or the myc tag. Both GFP- and myc-tagged Kif5A coimmunoprecipitated GFP-tagged and untagged Varp (left panel). Diamonds, Varp-GFP; stars, untagged Varp; arrowheads, GFP-Kif5A; circles, Kif5A-myc.

(D) Varp coprecipitates with Kif5A-ID (left panel). COS-7 cells were cotransfected with untagged Varp and GFP-Kif5A-ID or GFP as control. After 24 hr, proteins were extracted and immunoprepicipitation was performed by using monoclonal antibody against GFP. Dashes, GFP; stars, untagged Varp; open arrowheads, GFP-Kif5A-ID; L, lysate; S, supernatant.

(E and F) Kif5A-ID mainly localizes in dendrites and impairs axonal growth in hippocampal neurons. Rat hippocampal neurons were cotransfected at 2-DIV with GFP-Kif5A-ID, GFP-Kif5A (full-length), or GFP as control and RFP as reported gene. After 24 hr, neurons were fixed and labeled for GFP, RFP, and the dendritic marker MAP2 (not shown). (E) GFP-Kif5A-ID is excluded from the axon. Scale bar, 50 μm. (F) Quantification of the axonal length (arrowheads in E) in transfected neurons.

Table 1. siRNA Sequences

Species	Target Protein	Oligo Name	Target Sequence
Human	MACF1	MACF1	AGGATGCGTATCGACCAACAA
			CTCGATGGAATACATTGAATA
			CAGAACATTGACCGAGTTAAA
Human	GolginA4	GolginA4	CCGTGGAGTCTTTGTTTCGAA
			AAGGAGATGCAAGAAACGTTA
			CAGCAAAGAGTGAAGCGTCAA
Rat	Kif5A	Kif5A_r1	ATGGCGGAGACCAATAACGAA
Rat	Kif5A	Kif5A_r2	CTGCGTTGTGAGCTTCCTAAA

explained by the saturation of a limiting step due to constitutive activity of Rab21. Because Rab21-Q78L increased the proportion of TI-VAMP-containing vesicles moving toward the cell periphery, we predicted that Rab21-Q78L should increase the rate of exocytosis of TI-VAMP and the amount of TI-VAMP at the cell surface. To address this question, we switched to COS-7 cells, a model in which we previously characterized TI-VAMP's function in exocytosis (Alberts et al., 2006). COS-7 cells were cotransfected with myc-tagged mutants of Rab21 and TI-VAMP-pHluorin and imaged (live) or treated to assess surface staining. Rab21-Q78L increased the rate of TI-VAMP-pHluorin exocytosis compared to Rab21-WT and Rab21-T33N (Figures 4E and 4F; Movie S7). Furthermore, by measuring the ratio of cell surface TI-VAMP to the total amount in cells expressing Rab21 mutants, we showed a significant difference between Rab21-Q78L and Rab21-T33N (Figures 4G and 4H). Taken together, these results show that Rab21 activation enhances anterograde transport and exocytic activity of TI-VAMP. This suggests that Rab21 controls TI-VAMP anterograde flux and thereby its availability at the cell periphery to mediate exocytosis.

Varp and Rab21 Partners, GolginA4 and MACF1, Regulate Golgi to Periphery Transport of TI-VAMP Vesicles

It is widely accepted that Rab GTPases regulate membrane traffic through the recruitment and activation of effectors, which interact with their GTP-bound forms (Grosshans et al., 2006; Stenmark, 2009). However, Rab21 mutants might also affect the motility of TI-VAMP vesicles through posttranslational modification (PTM) of MTs, such as acetylation and tyrosination. Indeed it has been shown that PTMs affect the binding and the dynamics of some kinesins (Bulinski, 2007; Konishi and Setou, 2009; Reed et al., 2006). We did not find any significant difference in either the distribution or the amount of these two PTMs in HeLa or in differentiated PC12 cells expressing Rab21 mutants (Figures S4A–S4C). Furthermore, the dynamics of the MT plus-end tracking protein EB3 was not affected by the expression of the Rab21 mutants (Figures S4D and S4E), suggesting that Rab21 modulates TI-VAMP vesicles dynamics without significantly modifying the integrity and dynamics of the MT network.

In a Y2HS using the Rab21 constitutively active (Q78L) form as bait and a fetal brain library, we identified the spectraplakin microtubule actin cross-linking factor (MACF1) with an ID located within the tail spectrin repeats (Figure 5A). MACF1, also called ACF7 (Lin et al., 2005), is essential for MT dynamics (Kodama et al., 2003). Strikingly, we also found GolginA4 (also known as t-Golgin1 and p230), a membrane tether involved in Golgi positioning (Yoshino et al., 2005), as an additional partner of Varp with an ID located in the central coiled-coil domain (Figure 5B). Interestingly, GolginA4 interacts with MACF1, and both are involved in the transport of GPI-anchored proteins from Golgi to cell periphery (Kakinuma et al., 2004). Using the 3-aminotriazole stringency test in Y2H, we found that Varp/GolginA4 interaction was as strong as the gold standard Smad3/Smurf1 interaction (Colland et al., 2004), whereas the Rab21-Q78L/MACF1 interaction was slightly weaker (Figure S5A). To validate these interactions in mammalian cells, COS-7 cells were cotransfected with a GFP-tagged-MACF1-interacting region (GFP-MACF1-ID) and the three myc-tagged forms of Rab21. Interestingly, MACF1-ID interacted both with Rab21-WT and Rab21-Q78L but not with Rab21-T33N, suggesting that MACF1 is an effector of Rab21 (Figure 5C, left). We further confirmed the interaction by coimmunoprecipitating Rab21-Q78L with endogenous MACF1 in COS-7 cells (Figure 5D). The localization of endogenous MACF1 in COS-7 cells overexpressing either Rab21-Q78L or Rab21-T33N was then analyzed using a specific antibody recognizing both MACF1A and B isoforms or only the B isoform (Lin et al., 2005). In these cells MACF1A/B localized in the perinuclear region as previously described and overlapped significantly in vesicular-like structures with Rab21-Q78L (Figures 5E and 5F) but was juxtaposed more than overlapping with the GDP-locked Rab21-T33N form (Figure 5G; Rab21 to MACF1 staining overlap in the perinuclear region: 54.14% ± 2.31% for Rab21-Q78L and 44.64% ± 2.97% for Rab21-T33N, $p < 0.05$, Student's t test). Moreover, Rab21-Q78L and MACF1 overlapped along tubulin-positive tubular structures emanating from the perinuclear region (Figure S5B). We further demonstrated the interaction of Varp with GolginA4 by showing coimmunoprecipitation of endogenous GolginA4 and Varp-GFP (Figure 5H) and by using the ID of GolginA4 fused to GFP (GFP-GolginA4-ID) as bait (Figure 5I). Golgins and their interacting partners maintain Golgi structure and may act as matrix components (Barr and Short, 2003; Goud and Gleeson, 2010). Selectively silencing Varp expression by siRNA in HeLa cells as described previously (Burgo et al., 2009), induced a dispersion of GolginA4 staining compare to control cells (Figure 5J). To quantify the effect of siRNA Varp on GolginA4 structures dispersion, we measured the area of GolginA4

(G) Kif5A-ID impairs TI-VAMP accumulation at the growth cone. Rat hippocampal neurons were transfected at 2-DIV with GFP-Kif5A-ID, GFP-Kif5A, or GFP as control. After 24 hr, neurons were fixed and labeled for GFP, TI-VAMP, and MAP2 (shown only in the overlay images, blue). The density of TI-VAMP staining was compared between cell body and growth cone (arrowheads) from the same neurons. Scale bars, 20 μm.
(H) Ratio of fluorescent density of TI-VAMP staining between the growth cone and cell body. All data in this figure are shown as mean ± SEM. Significance is determined by one-way ANOVA, Dunnett's posttest. *$p < 0.05$, ***$p < 0.001$.
See also Figure S2.

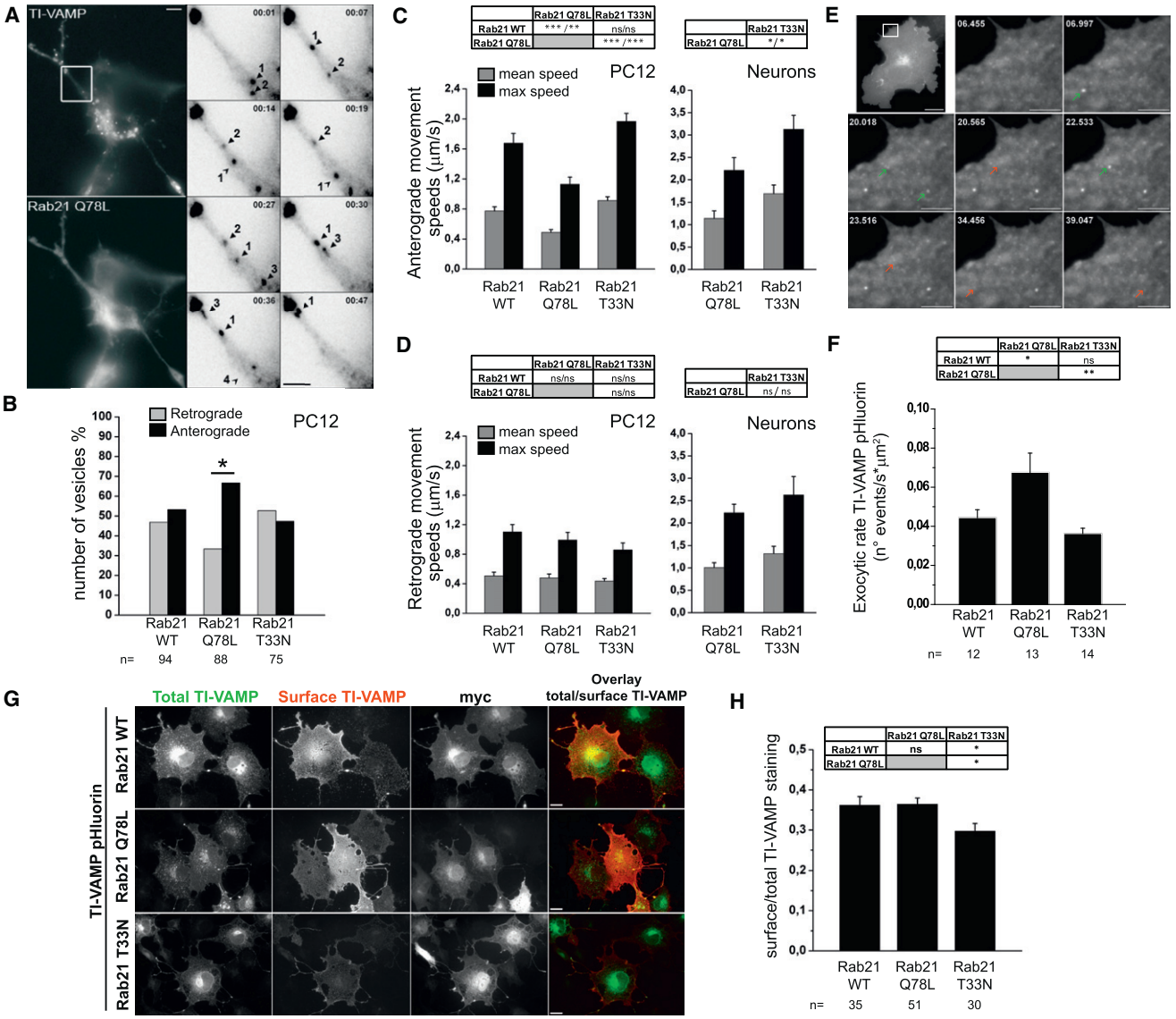

Figure 4. Rab21 Regulates TI-VAMP Traffic and Exocytosis

(A) Anterograde and retrograde movements of RFP-TI-VAMP vesicles were tracked in GFP-Rab21-expressing PC12 cells. Anterograde (full arrowhead) and retrograde (open arrowhead) vesicular movements of RFP-TI-VAMP vesicles are shown in the series of frames (right panels; scale bar, 5 μm) corresponding to a magnification of the boxed region in GFP-Rab21-Q78L-expressing cells (top left; scale bar, 10 μm; see Movie S6; min:sec).

(B) Quantification of TI-VAMP anterograde- versus retrograde-moving vesicles along the neurites. Significance determined by two-tailed Fisher's test, *$p < 0.05$. n = number of TI-VAMP vesicles analyzed. Quantification of the anterograde (C) and retrograde (D) RFP-TI-VAMP-tagged vesicle mean (excluding the pausing times) and max speeds in the corresponding transfection conditions in PC12 cells (left panels) and young rat hippocampal neurons (right).

(E) COS-7 cells were cotransfected with TI-VAMP-pHluorin and myc-tagged Rab21 mutants (ratio cDNAs 1:3) and imaged after 16–24 hr. Snapshots from Movie S7 show exocytic (green arrows) and endocytic (red arrows) events of TI-VAMP-pHluorin. Scale bars, 20 and 5 μm (Inset).

(F) Quantification of the density per sec of TI-VAMP-pHluorin exocytosis. n, number of cells. (G) TI-VAMP-pHluorin surface versus total staining in COS-7 cells cotransfected with Rab21-myc-tagged mutants. Scale bars, 20 μm.

(H) Quantification of the ratio between TI-VAMP-pHluorin surface and total staining in Rab21-myc-tagged-expressing cells (see Experimental Procedures). n, number of cells. Data are shown as mean ± SEM. Significance is determined by one-way ANOVA, Tukey's posttest. *$p < 0.05$, **$p < 0.01$, ***$p < 0.001$.

See also Figures S3 and S4 and Movies S5, S6, and S7.

staining in the siRNA-treated HeLa cells. Silencing Varp with two different oligonucleotides (Varp_h1 and Varp_h2) induced a significant increase of the GolginA4 staining area compared to control conditions (scrambled siRNA and mock transfection). The effect on GolginA4 dispersion was correlated with the degree of silencing of the two oligonucleotides, thus supporting the specificity of the effect (Figures 5K and 5L). In summary, we have demonstrated that MACF1 preferentially interacts and colocalizes with Rab21 locked in the active GTP-bound form and that GolginA4, a molecular partner of MACF1, interacts

with Varp to mediate correct Golgi localization. These results suggest that Varp, Rab21, GolginA4, and MACF1 may play a role in regulating TI-VAMP's Golgi sorting.

To provide insight into the function of MACF1 and GolginA4, we investigated their role on axonal growth in hippocampal neurons and on sorting of nascent TI-VAMP vesicles from the Golgi apparatus. To this end, we relied on both expression of IDs and selective silencing (Table 1) of the expression of MACF1 and GolginA4. Both MACF1-ID and GolginA4-ID significantly impaired axonal growth (Figures 6A and 6B), and combined expression of the two IDs together showed slightly stronger inhibition than each ID alone. MACF1 and GolginA4 are scaffolding TGN proteins (Goud and Gleeson, 2010; Lin et al., 2005), and we have shown previously that TI-VAMP-Varp-Rab21 colocalized mainly at the TGN (Burgo et al., 2009). Therefore, we tested if MACF1 and GolginA4 may control the sorting of TI-VAMP vesicles at the TGN by using a previously described method (Cao et al., 2005). Indeed, the transit of RFP-TI-VAMP cotransfected with GFP (control) was blocked in the TGN by incubation at 20°C for 3 hr, then released, and transported from the cell center to the periphery at 37°C (Figure 6C, left). Cells coexpressing GFP-MACF1-ID or GFP-GolginA4-ID (data not shown) showed a significant retention of nascent RFP-TI-VAMP protein in a tight perinuclear bolus after release of the temperature block (Figure 6C, right). Quantification of TI-VAMP staining from cell center to periphery in the different experimental conditions demonstrated that MACF1-ID, as well as GolginA4-ID to a lesser extent, impaired the sorting of nascent TI-VAMP (Figures 6D and 6E). Selective knockdown of endogenous GolginA4 (Figures 6G and 6H) and MACF1 (Figure 6I) similarly inhibited transport of TI-VAMP to the cell periphery (Figure 6F). The similar inhibition of TI-VAMP transport produced by ID expression and silencing strongly argues in favor of a role of both GolginA4 and MACF1 in TI-VAMP vesicles sorting at the TGN and transport to the cell periphery.

DISCUSSION

Here we report evidence that TI-VAMP is the starting point of a molecular network that promotes events that precede its involvement as a fusogenic "v-SNARE" protein and mediate its transport from the Golgi apparatus, in the cell center, to the cell periphery. Combining Y2HS and biochemical and functional approaches, we demonstrated that the Rab21 GEF Varp, a TI-VAMP partner, interacts both with GolginA4 and the kinesin1 Kif5A and that MACF1, a GolginA4 partner, is a Rab21 effector. We further showed here that Rab21, Kif5A, GolginA4, and MACF1 are involved in the transport of TI-VAMP from the cell center to the periphery and in particular to neurite tips. Previous results showed that TI-VAMP is blocked in the TGN in *mocha* neurons, which are deficient in AP-3 (Scheuber et al., 2006), and that TI-VAMP, Varp, and Rab21 colocalize in the TGN area (Burgo et al., 2009). Additionally, the inactive Rab21-T33N colocalizes with GolginA4 (Simpson et al., 2004), and MACF1B and GolginA4 localize in the TGN (Goud and Gleeson, 2010; Lin et al., 2005). Altogether, these data suggest that the TGN is the main site of action of Varp, Rab21, GolginA4, and MACF1. In addition, the molecular network we unraveled here connects TI-VAMP vesicles to MTs and MT-based anterograde transport. Indeed, TI-VAMP vesicles move anterogradely along MTs, with both their directionality and anterograde velocity regulated by the activity of Rab21. Furthermore, Varp binds the MT molecular motor Kif5A tail, and this interaction is involved in the transport of TI-VAMP to neuronal growth cones, and Rab21, in its GTP bound form, binds to MACF1, which interacts with MTs through its tail (GAR domain) (Sun et al., 2001). Taking into account the multiple molecular and functional connections between these proteins, we are able to propose a working hypothesis for the transport of TI-VAMP vesicles from the TGN to the cell periphery (Figure 7). The sorting of TI-VAMP into vesicles at the TGN would depend on its interaction with Varp, which in turn interacts with GolginA4 and activates Rab21, leading to its interaction with MACF1. MACF1 and GolginA4 interaction with Rab21-Q78L and Varp, respectively, suggests the occurrence of a dynamic molecular network. Next, Varp-Kif5A binding would mediate the loading of TI-VAMP vesicles onto MTs and their transport to the cell periphery. How these molecular interactions are precisely synchronized in time and space, particularly with the assembly and disassembly of the AP-3 coat (Scheuber et al., 2006), remains to be elucidated. Directing TI-VAMP to the cell periphery would then allow it to fulfill its function as a secretory v-SNARE (Danglot et al., 2010; this study), followed by endocytosis via Hrb, AP-2, and clathrin (Chaineau et al., 2008; Pryor et al., 2008), then to participate in early (Moreau et al., 2011) and late (Fader et al., 2009) phases of autophagy, lysosomal degradation (Pryor et al., 2004), and finally to mediate secretion of lysosomes (Chaineau et al., 2009; Proux-Gillardeaux et al., 2007).

The present study also further extends the general concept that Rab GTPases are involved in sorting and transport of intracellular vesicles. In particular, Rab6, a Golgi-associated Rab, forms a complex with myosin II and controls the fission of Rab6 and VSV-G-containing vesicles (Miserey-Lenkei et al., 2010). Rab 6 and 8 further control the transport of constitutive SVs to the cell periphery, as well as their docking and fusion (Grigoriev et al., 2007, 2011). Furthermore, Rab27A mediates anterograde kinesin I-dependent transport of SV (Arimura et al., 2009), its effector MyRIP controls the motion of secretory granules (Desnos et al., 2003), and protrudin/Kif5 interaction is involved in Rab11 transport (Matsuzaki et al., 2011). It is thus likely that, as for the maturation of endosomes (Rink et al., 2005), the secretory pathway utilizes a chain of Rab proteins acting sequentially to guide and deliver secretory vesicles to their proper destination within the cell. SNAREs and particularly TI-VAMP appeared very early in evolution (Kloepper et al., 2008), and thus it is tempting to envision coevolutionary mechanisms allowing for the occurrence of molecular networks organized around SNAREs to ensure their proper delivery within cells. In conclusion, we propose that the v-SNARE TI-VAMP is the starting point of a dynamic molecular network involved in its targeting to allow for its secretory and downstream functions.

EXPERIMENTAL PROCEDURES

Yeast Two-Hybrid Analysis

The coding sequence for full-length human Varp was PCR-amplified and cloned into pB29 as an N-terminal fusion to LexA. Human Q78L ΔCAAX Rab21 (amino acids 1–220) was cloned by PCR into pB6 as a C-terminal fusion to Gal4 DNA-binding domain. The constructs were used as baits to screen

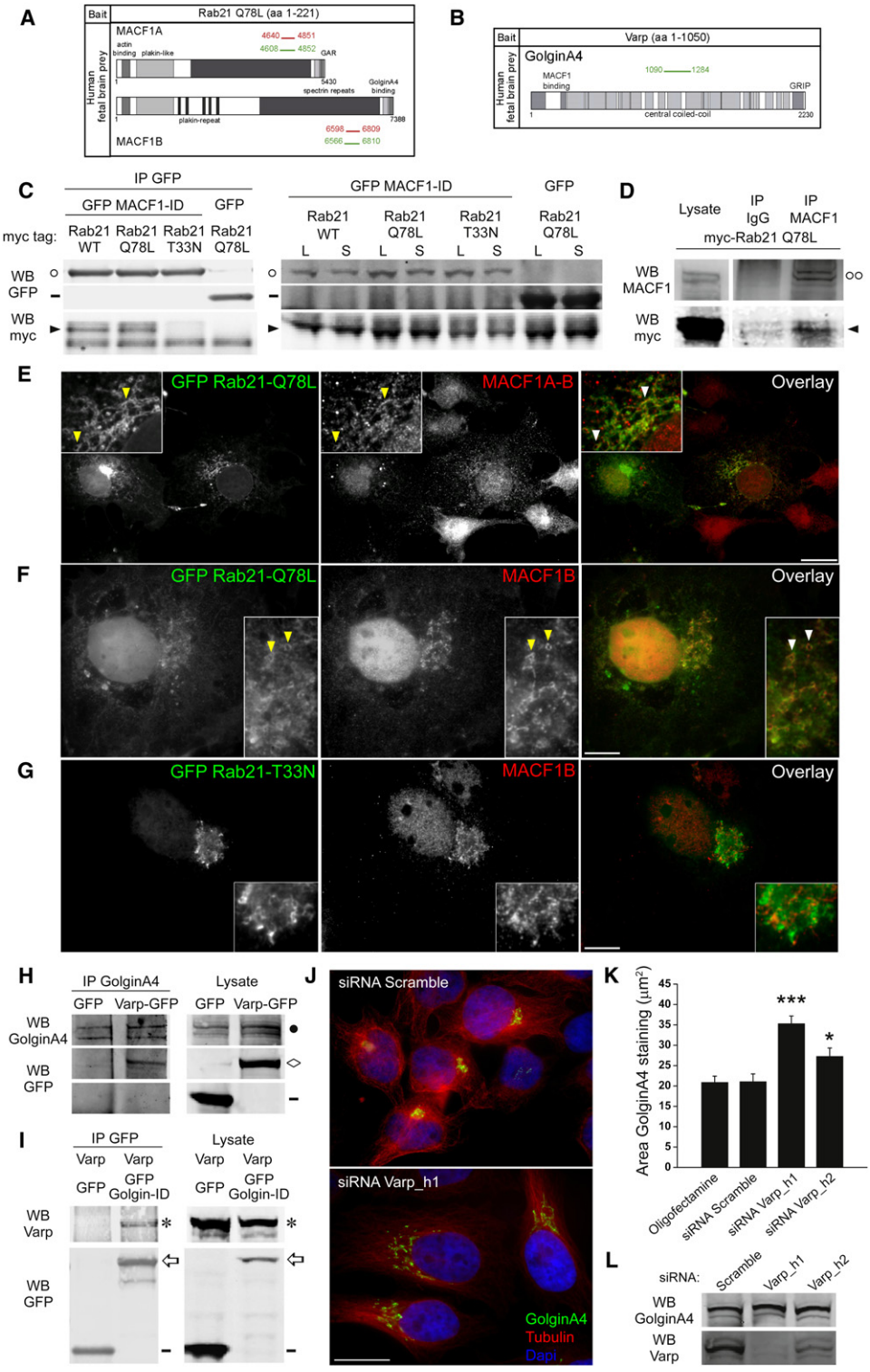

Figure 5. MACF1 and GolginA4 Interact with Rab21 and Varp

(A) MACF1A-B were identified as partners of Rab21-Q78L in an Y2HS using the full-length protein as bait and the human fetal brain cDNA library. Green lines highlight the total coverage of all prey clones identified in the screens, and red lines represent the intersection of the clones (common to both MACF1A and B). GAR, MT binding domain.

(B) GolginA4 was identified as partner of Varp in Y2HS using full-length Varp as a bait in a human fetal brain cDNA library.

(C) GFP-MACF1-ID coimmunoprecipitates with Rab21-WT and Rab21-Q78L but not with Rab21-T33N (left). COS-7 cells were cotransfected with the Rab21-WT, Rab21-Q78L, or Rab21-T33N-myc and GFP-MACF1-ID or GFP as control. Immunoprepicipitation was performed by using monoclonal antibody against GFP.

at saturation a highly complex random-primed human fetal brain domain library. For Varp, 106 million clones (10-fold the complexity of the library) were screened using a mating approach with Y187 (matα) and L40ΔGal4 (mata) yeast strains as previously described (Fromont-Racine et al., 1997). His+ colonies were grown on a medium lacking tryptophan, leucine, and histidine, supplemented with 0.5 mM 3-aminotriazole and 165 were selected. For Rab21-Q78L, 116 million clones were screened using the same mating approach with Y187 (matα) and CG1945 (mata) yeast strains. His+ colonies were selected on a medium lacking tryptophan, leucine, and histidine, supplemented with 0.5 mM 3-aminotriazole and 26 were selected. The prey fragments of the positive clones were amplified by PCR and sequenced at their 5′ and 3′ junctions. The resulting sequences were used to identify the corresponding interacting proteins in the GenBank database (NCBI), using a fully automated procedure. Briefly, 5′ and 3′ sequences were filtered by using PHRED. Sequence contigs were built using CAP3 and compared to the latest release of GenBank using BLASTN (Formstecher et al., 2005). In the Varp screen, one KIF5A fragment and one GolginA4 fragment were identified. In the Rab21 screen, a total of seven clones coded for MACF1 fragments, corresponding to two distinct fusions (six clones for aa 4608–4852 of MACF1A and one clone for aa 4640–4851).

Cell Culture and cDNA Transfection

HeLa and COS-7 cells were grown in Dulbecco's modified Eagle's medium (DMEM) (GIBCO, Invitrogen, Cergy-Pontoise Pointoise, France) containing 10% (v/v) fetal bovine serum (PAA Laboratories Inc., Dartmouth, MA), 10 units/ml penicillin, and 10 μg/ml streptomycin, in a 5% CO_2-humidified atmosphere at 37°C. PC12 cells were maintained in RPMI 1640 (GIBCO, Invitrogen) medium containing 10% (v/v) horse serum (Invitrogen) and 5% fetal bovine serum on collagen-coated dishes. PC12 cells were differentiated with h-NGF at 50 ng/ml for 3–4 days. Cells were transfected with Lipofectamine 2000 (Invitrogen) as described by the supplier. Cells were fixed after 16–24 hr with 4% paraformaldehyde (PFA) and processed for immunofluorescence microscopy as described previously (Martinez-Arca et al., 2000). Hippocampal neurons from embryonic rats (E19) were prepared as described previously (Danglot et al., 2003) and grown on polyornithine-coated (Sigma-Aldrich, Saint Quentin Fallavier, France) either 14 or 30 mm coverslips at a density of 100,000 and 500,000, respectively, in Neurobasal media, supplemented with 2% B27, 2 mM L-glutamine. Neurons were transfected at 2-DIV by using Lipofectamine 2000 in accordance with the manufacturer's instructions. After 16–24 hr, neurons were fixed with 4% PFA and processed for immunofluorescence.

STICS Analysis

A custom code in MATLAB 7 (The MathWorks) was written to perform the STICS analysis on 15 min interval nonoverlapping 25-frame time windows as previously described (Hebert et al., 2005; Wiseman et al., 2004). Mean TI-VAMP STICS velocities were obtained by averaged STICS velocities calculated in several selected regions (6–11) all along the cells and at each time point.

Axonal Length Assay and v-SNARE Distribution Quantification

For axonal length assay in rat hippocampal neurons, between 30 and 70 transfected neurons were randomly selected and the axon, defined as the longest and MAP2 negative neurite, was measured by using MetaMorph software (Roper Scientific, Evry, France). Each experiment was repeated three to four times with similar results. Statistical significance was determined by using GraphPad PRISM 5 software. For TI-VAMP and Synaptobrevin2 localization assays, we projected the maximum values of confocal acquisitions and plotted the gray values on an axis drawn from inside the nucleus to outside the cell. To avoid x-y variability, we integrated the measured gray values on a 10-pixel-width band. We normalized both the length and the fluorescence intensity by homothetic transformations, resulting in the distribution of gray values as percent of total intensity on a 100-pixel-long axis, where zero is the end of the nucleus (defined as the region where the mean intensity of three adjacent pixels is multiplied by two) and 100 is the end of the cell (defined as "gray value below 8," which corresponds approximately to background intensity).

Immunoprecipitation and Immunoblot Assays

Immunoprecipitation experiments were carried out as previously described (Martinez-Arca et al., 2003). Briefly cells were lysed in TSE (50 mM TrisHCl [pH 8.0], 150 mM NaCl, and 1 mM EDTA) plus 1% Triton ×100 and 1.2 mg of protein extract was submitted to immunoprecipitation overnight at 4°C, with 25 μl of Protein-G- or -A-coupled Sepharose beads (GE Healthcare, Waukesha, WI, USA) previously cross-linked with the specific antibody. After specific wash, bound proteins were eluted by loading the beads with SDS sample buffer and subjected to SDS-PAGE analysis by using NuPAGE 4%–12% Bis-Tris or NuPAGE Tris-Acetate gradient gels (Applied Biosystems, Cergy Pontoise, France). Gels were transferred onto nitrocellulose filters (Protran; Schleicher and Schuell, Dassel, Germany) and then processed for western blotting. Membranes were pretreated with 5% nonfat dry milk and 0.1% Tween 20 in 200 mM Tris and 0.15 M NaCl (TBS) (pH 7.3 [TBS-T]) followed by incubation with the primary antibodies overnight. After washing in T-TBS, the membranes were blotted with secondary antibodies (goat anti-rabbit or anti-mouse IR dye 680 and goat anti-mouse or anti-rabbit IR dye 800 purchased from Molecular Probes, Applied Biosystems, and Rockland Immunochemicals, Gilbertsville, PA, USA, respectively). Detection was carried out by the infrared imaging system Odyssey of LI-COR Biosciences (Lincoln, NE, USA). Alternatively, the membranes were blotted with secondary antibodies coupled to HRP, and detection was carried out by chemiluminescent assay (SuperSignal West Femto Maximum Sensitivity Substrate, Thermo Scientific).

Time-Lapse Imaging, v-SNARE pHluorin Analysis, and Vesicles Tracking

Optical recordings were performed between 16–24 hr after transfection. In dual-color imaging time-lapse experiments, channels were collected sequentially every 4–5 s, using an inverted microscope Leica DMI6000B (Leica Microsystem, Manheimm, Germany) equipped with a high-pressure mercury arc lamp (HBO 100W, Osram), a 63×/1.4 NA Plan-Apochromat oil-immersion Leica objective, a 1.6× tube lens with 497 to 557 nm emission, a 505 nm dichroic filters, and a digital camera (Cascade:512B; Roper Scientific, Trenton, NJ, USA). For pHluorin acquisition, images were recorded every 0.5 s over a time period of 3 min, by using a 488-Ar^+ ion acousto-optically shuttered laser whose beam was expanded to fill the field of view. Imaging was conducted

(D) Endogenous MACF1 coimmunoprecipitates Rab21-Q78L-myc in COS-7 cells. Circle, GFP-MACF1-ID; dash, GFP; arrowhead, Rab21-myc; double circle, endogenous MACF1; L, lysate; S, supernatant.
(E–G) Rab21-Q78L, but not Rab21-T33N, staining overlaps with MACF1 in Golgi stacks and vesicular structures. COS-7 cells were transfected with GFP-Rab21-Q78L or -T33N, fixed, and labeled after 16 hr for GFP and MACF1A and B (E) or only MACF1B (F–G).
(H) Varp-GFP coimmunoprecipitates with endogenous GolginA4 in COS-7 cells.
(I) Varp coprecipitates with GolginA4-ID. COS-7 cells were cotransfected with untagged Varp and GFP-GolginA4-ID or GFP as control. Immunoprepicipitation was performed using monoclonal antibody against GFP (left). Full circle, endogenous GolginA4; diamond, Varp-GFP, star, untagged Varp; arrow, GFP-GolginA4-ID; dash, GFP.
(J) Varp regulates GolginA4 perinuclear localization. HeLa cells were transfected with scrambled siRNA or two Varp siRNAs (Varp_h1, Varp_h2). After 72 hr, cells were fixed and stained for GolginA4 (green), β-tubulin (red), and DAPI (blue).
(K) Quantification of the area of the GolginA4 staining in Varp and scrambled siRNA-treated cells. Data are shown as mean ± SEM. Significance is determined by one-way ANOVA, Tukey's posttest. *$p < 0.05$, ***$p < 0.001$.
(L) Western blot showing the efficiency of Varp silencing in HeLa cells. Total amount of GolginA4 protein is not affected by silencing Varp. Scale bars, 20 μm.
See also Figure S5.

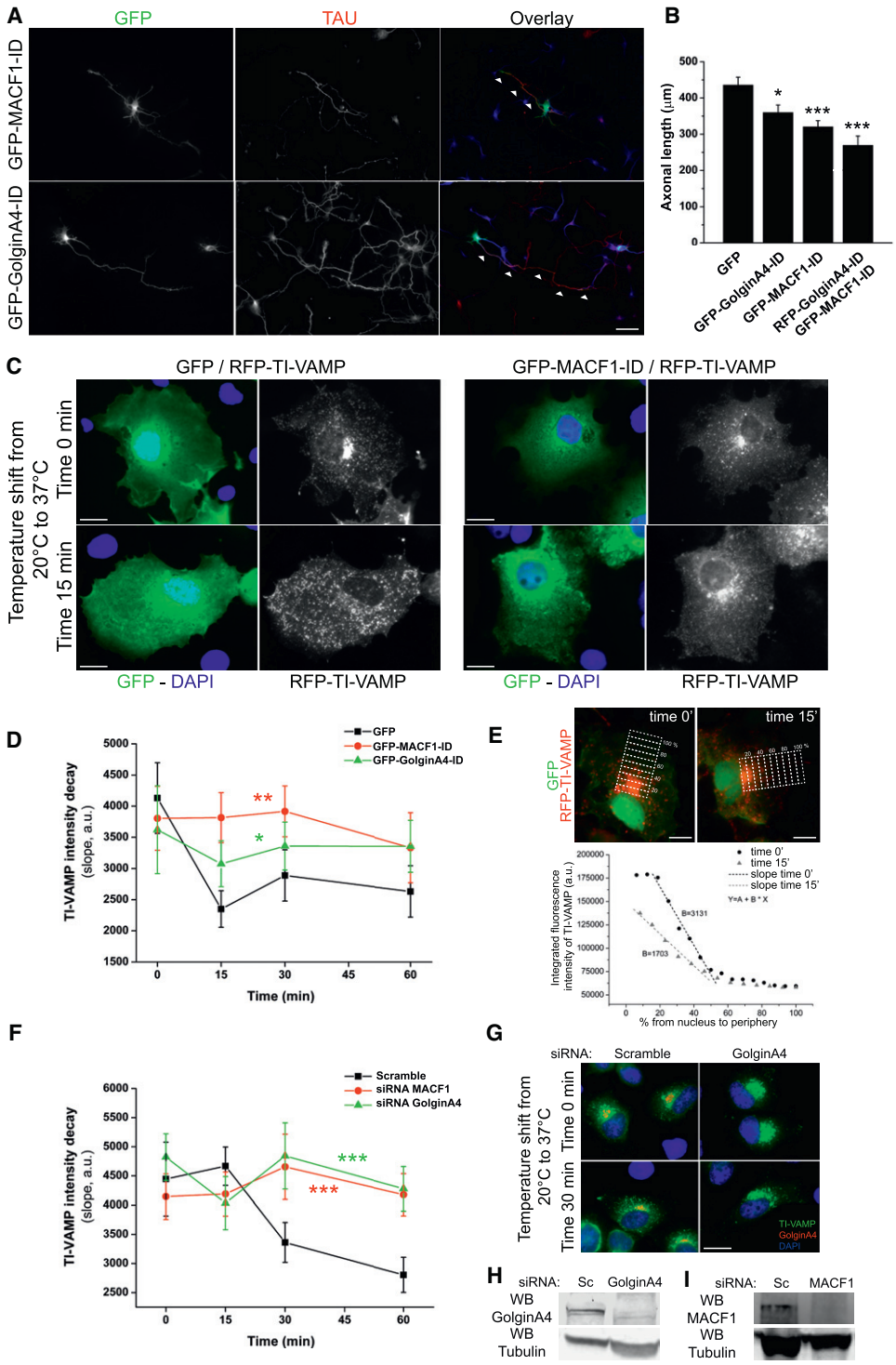

Figure 6. MACF1 and GolginA4 Regulate Axonal Growth and Sorting of Nascent TI-VAMP Vesicles

(A–B) MACF1-ID and GolginA4-ID impair axonal growth. (A) Rat hippocampal neurons were transfected at 2-DIV with GFP-MACF1-ID, GFP-GolginA4-ID, or GFP as control. Neurons were also cotransfected with GFP-MACF1-ID and RFP-GolginA4-ID (not shown). After 24 hr, neurons were fixed and labeled for GFP, axonal (TAU), and dendritic (MAP2, blue staining showed only in the overlay) markers. Scale bars, 50 μm. (B) Quantification of axonal length (arrowheads in A) in the different experimental conditions. Data are shown as mean ± SEM. Significance is determined by one-way ANOVA, Tukey's posttest, *$p < 0.05$, ***$p < 0.001$.

(C–E) MACF1-ID and GolginA4-ID alter the trafficking of TI-VAMP from perinuclear region to periphery. (C) COS-7 cells were cotransfected with RFP-TI-VAMP and either GFP-MACF1-ID or GFP-GolginA4-ID or GFP as control. Following 16 hr posttransfection, cells were incubated at 20°C for 3 hr, allowed to accumulate the nascent RFP-TI-VAMP protein at the perinuclear region, and then warmed to 37°C for 15, 30, or 60 min. Alleviation of the temperature block by shifting the

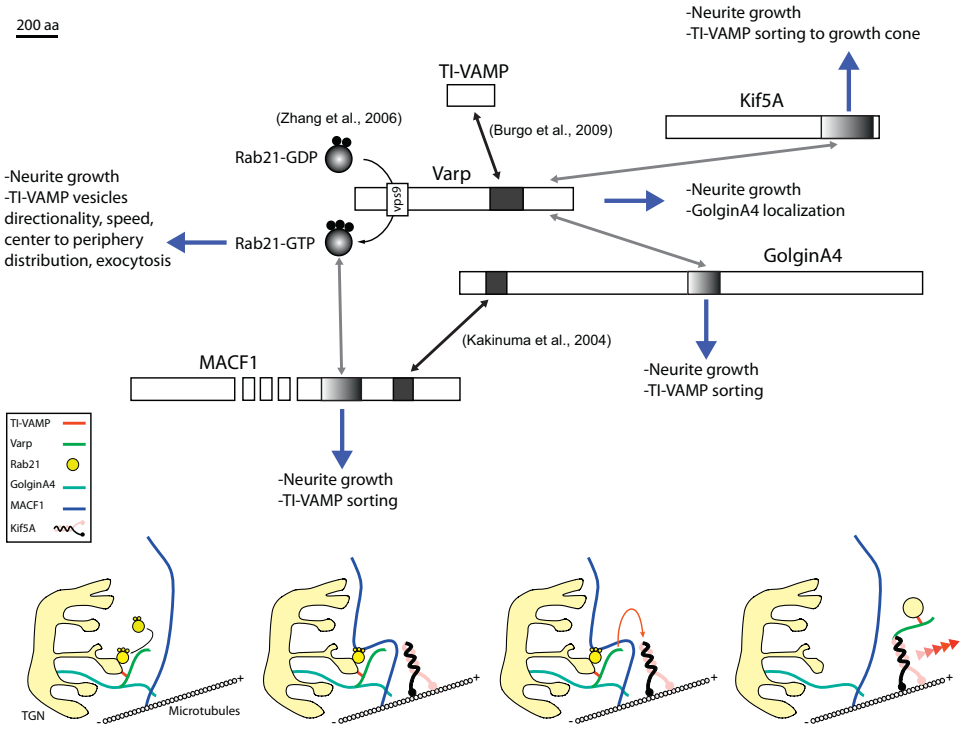

Figure 7. Molecular Network Mediating the Transport of TI-VAMP from Cell Center to Periphery: Function of Each Component, Interactions and Working Hypothesis

Based on the present results and cited publications, we propose that the sorting of TI-VAMP vesicles from the TGN depends on its interaction with Varp, which in turn interacts with GolginA4 and activates Rab21, leading to its interaction with MACF1. These sequential interactions would position budding vesicles containing the TI-VAMP/Varp complex for interaction with Kif5A. Next, Varp/Kif5A binding would mediate the loading of TI-VAMP vesicles onto MTs and their transport to the cell periphery, allowing for TI-VAMP function in exocytosis.

in modified Krebs-Ringer-HEPES buffer (135 mM NaCl, 2.5 mM KCl, 1.2 mM MgCl, 1 or 2 mM $CaCl_2$, 20 mM HEPES, 11.1 mM glucose, and pH 7.4). Acidic solution with final pH of 5.5 was prepared by replacing HEPES with MES (pK_a = 6.1); all other components remaining unchanged. Ammonium chloride solution (pH 7.4) was prepared by substituting 50 mM NaCl in the above saline with NH_4Cl; all other components remained unchanged (Sankaranarayanan et al., 2000). Temperature was controlled by warmed air (37°C). The power source and exposure time were the lowest possible (20%–30%) to avoid phototoxicity. Transient exocytic events of TI-VAMP- and Syb2- pHluorin in hippocampal neurons and COS-7 cells were manually counted by using the ImageJ plugin Point Picker and related to the analyzed cell surface area (expressed in μm^2) and the time of recording (180 s). Alternatively, to analyze the effect of pH on TI-VAMP-pHluorin fluorescence, images of neurons were analyzed by using the MetaMorph software. First, we generated a kymograph picture, and then the kymograph result was segmented and line-scanned, resulting in the projection of the intensity of fluorescence over the time.

RFP-TI-VAMP vesicle motility in differentiated PC12 cells coexpressing GFP-Rab21 mutants was quantified using the Manual Tracking plugin, available on the ImageJ website (http://rsb.info.nih.gov/ij/plugins/track/track.html). Statistical significance was determined by using GraphPad PRISM 5 software.

Surface Immunostaining of TI-VAMP-pHluorin in COS-7 Cells

Surface immunostaining of COS-7 cells was performed 16–24 hr after transfection. Briefly, cells were washed at 4°C with DMEM buffered with 20 mM HEPES and then incubated 5 min at 4°C with mouse mAb anti-GFP. After extensive washing, cells were fixed and incubated with a Cy3-coupled secondary antibody. Cells were then permeabilized and processed for immunofluorescence using the same primary antibody and the Alexa Fluor 488-coupled secondary antibody. This protocol allowed to distinguish the fraction of TI-VAMP expressed at the surface (Cy3 staining) and the total amount of expressed protein (Alexa-488 staining). For the quantification of the integrated fluorescence intensity, a minimum of 15 TI-VAMP-pHluorin-positive cells coexpressing myc-tagged Rab21 mutants were considered for each condition and the ratio between surface / total integrated signal was measured for each cell. Statistical significance was determined by using GraphPad PRISM 5 software.

cells to 37°C stimulated the traffic of nascent RFP-TI-VAMP protein from the perinuclear region to a more peripheral distribution in cells expressing GFP (left panels), whereas cells expressing GFP-MACF1-ID (right panels) or GFP-GolginA4-ID (not shown) retained a compacted bolus of RFP-TI-VAMP at the perinuclear region (bottom right).

(D and E) The amount of RFP-TI-VAMP vesicles trapped within the perinuclear region was calculated by measuring the decay of RFP-TI-VAMP fluorescence intensity (slope, B) from perinuclear to peripheral region (see Experimental Procedures).

(F–I) Silencing MACF1 and GolginA4 decrease the traffic of TI-VAMP from the perinuclear region to periphery. HeLa cells were transfected either with scrambled or MACF1 or GolginA4 siRNAs. After 72 hr, cells were transfected with GFP-TI-VAMP and processed after 24 hr as described in (C). (F) Quantification of the effects of MACF1 and GolginA4 silencing on TI-VAMP distribution from cell center to periphery. (G) Example of blockage of TI-VAMP in GolginA4-silenced cells. (H–I) Western blot showing the efficiency of GolginA4 and MACF1 silencing in HeLa cells. All data in this figure are shown as mean ± SEM. Significance is determined by two-way ANOVA, *$p < 0.05$, **$p < 0.01$, ***$p < 0.001$. Scale bars, 20 μm.

siRNA Knockdown

Varp RNA interference in HeLA cells was achieved by using two sets of specifics predesigned siRNA duplexes previously described (Burgo et al., 2009). MACF1 and GolginA4 RNA interferences in HeLa cells were achieved by using specific predesigned siRNA duplexes (QIAGEN, Courtaboeuf, France, see Table 1). A nontargeting siRNA (scramble) and mock transfection were used as controls. Human HeLa cells were transfected twice with oligonucleotides at a concentration of 30–50 nM by using oligofectamine (Invitrogen) in accordance with the manufacturer's instructions and cultured for additional 72–96 hr. Cells were treated for western blot analysis to assess the efficiency of siRNA treatment or plated on uncoated 12 mm diameter coverslips, fixed, and processed for immunofluorescence. Between 27 and 40 randomly chosen cells were analyzed, and the area of GolginA4 antibody staining was measured after thresholding by using MetaMorph software. Showed data are representative of four analogous experiments with similar results. In TI-VAMP transport assay HeLa cells were transfected after 72 hr from the first siRNA transfection with GFP-TI-VAMP and processed for immunofluorescence after 24 hr. Between 20 and 40 nondividing cells were considered for each time point and in each experimental condition and analyzed as described previously. Kif5A RNA interference in rat hippocampal neurons was achieved by using specific predesigned siRNA duplexes (QIAGEN, Courtaboeuf, France; see Table 1). Neurons were cotransfected at 2-DIV with oligonucleotides at concentration of 100 nM and 0.25 μg of EGFP by using Lipofectamine 2000 in accordance with the manufacturer's instructions and cultured for additional 48–72 hr. Neurons were then fixed with 4% paraformaldehyde and processed for immunofluorescence. TI-VAMP staining intensity was measured in 20–40 GFP-expressing neurons in each siRNA treatment. Statistical significance was determined by using GraphPad PRISM 5 software.

TI-VAMP Transport Assay

For detection of TI-VAMP transport from the cell center to the periphery, COS-7 cells were cotransfected for 16 hr with RFP-TI-VAMP and GFP-MACF1-ID, GFP-GolginA4-ID, or GFP as control. HeLa cells were transfected with GFP-TI-VAMP and corresponding siRNA (see siRNA Knockdown section and Table 1). Cells were then shifted to 20°C for 3 hr to block nascent FP-TI-VAMP in the Golgi compartment. Following the 20°C Golgi block, 100 μg/ml cycloheximide was added for 30 min. Cells were subsequently shifted to 37°C to induce release of FP-TI-VAMP and fixed after 15, 30, or 60 min. Images were acquired with fluorescence microscopy. The distribution of FP-TI-VAMP vesicles in the different experimental conditions was calculated using MetaMorph software by designing a grid from the nucleus (defined from the edge of DAPI staining) to the cell leading edge. The fluorescence intensity of FP-TI-VAMP was plotted in function of the distance from nucleus to periphery and the slope of the fluorescence decay was measured by using Microcal Origin software. Between 15 and 30 nondividing cells were considered for each time point and in each experimental condition.

ACCESSION NUMBERS

The protein interactions from this publication have been submitted to the IMEx (http://www.imexconsortium.org/) consortium through IntAct (pmid 22121220) and assigned the identifier IM-17311.

SUPPLEMENTAL INFORMATION

Supplemental Information includes five figures, Supplemental Experimental Procedures, and seven movies and can be found with this article online at doi:10.1016/j.devcel.2012.04.019.

ACKNOWLEDGMENTS

We are grateful to Catherine Dargemont, Marie-Christine Simmler, and Cathy Jackson for critical reading of the manuscript. We are grateful to Liu JunJun and Jorand Raphaël for help in performing STICS analysis. We are grateful to the Galli laboratory for helpful discussions and Giuseppe Baldacci for support. Work in our group was funded in part by grants from INSERM, the Association Française contre les Myopathies (AFM), the Association pour la Recherche sur le Cancer (ARC), the Mairie de Paris Medical Research and Health Program, the Fondation pour la Recherche Médicale (FRM), and the Ecole des Neurosciences de Paris (ENP) (to T.G.). A.B. was supported by FRM and AFM. E.F. is an employee and shareholder of Hybrigenics. Respecting the legal and ethical national requirements and code of practice is controlled at the Jacques Monod Institute by the Committee for Research and Ethical Issues Buffon referenced CEEA40 by the Ministère de la Recherche et de l'Enseignement Supérieur. Animal experiments were performed according to the governmental guidelines n°86/609/CEE.

Received: November 18, 2011
Revised: March 12, 2012
Accepted: April 16, 2012
Published online: June 14, 2012

REFERENCES

Advani, R.J., Yang, B., Prekeris, R., Lee, K.C., Klumperman, J., and Scheller, R.H. (1999). VAMP-7 mediates vesicular transport from endosomes to lysosomes. J. Cell Biol. *146*, 765–776.

Alberts, P., Rudge, R., Hinners, I., Muzerelle, A., Martinez-Arca, S., Irinopoulou, T., Marthiens, V., Tooze, S., Rathjen, F., Gaspar, P., and Galli, T. (2003). Cross talk between tetanus neurotoxin-insensitive vesicle-associated membrane protein-mediated transport and L1-mediated adhesion. Mol. Biol. Cell *14*, 4207–4220.

Alberts, P., Rudge, R., Irinopoulou, T., Danglot, L., Gauthier-Rouvière, C., and Galli, T. (2006). Cdc42 and actin control polarized expression of TI-VAMP vesicles to neuronal growth cones and their fusion with the plasma membrane. Mol. Biol. Cell *17*, 1194–1203.

Arimura, N., Kimura, T., Nakamuta, S., Taya, S., Funahashi, Y., Hattori, A., Shimada, A., Ménager, C., Kawabata, S., Fujii, K., et al. (2009). Anterograde transport of TrkB in axons is mediated by direct interaction with Slp1 and Rab27. Dev. Cell *16*, 675–686.

Barr, F.A., and Short, B. (2003). Golgins in the structure and dynamics of the Golgi apparatus. Curr. Opin. Cell Biol. *15*, 405–413.

Bulinski, J.C. (2007). Microtubule modification: acetylation speeds anterograde traffic flow. Curr. Biol. *17*, R18–R20.

Burgo, A., Sotirakis, E., Simmler, M.C., Verraes, A., Chamot, C., Simpson, J.C., Lanzetti, L., Proux-Gillardeaux, V., and Galli, T. (2009). Role of Varp, a Rab21 exchange factor and TI-VAMP/VAMP7 partner, in neurite growth. EMBO Rep. *10*, 1117–1124.

Cao, H., Weller, S., Orth, J.D., Chen, J., Huang, B., Chen, J.L., Stamnes, M., and McNiven, M.A. (2005). Actin and Arf1-dependent recruitment of a cortactin-dynamin complex to the Golgi regulates post-Golgi transport. Nat. Cell Biol. *7*, 483–492.

Chaineau, M., Danglot, L., Proux-Gillardeaux, V., and Galli, T. (2008). Role of HRB in clathrin-dependent endocytosis. J. Biol. Chem. *283*, 34365–34373.

Chaineau, M., Danglot, L., and Galli, T. (2009). Multiple roles of the vesicular-SNARE TI-VAMP in post-Golgi and endosomal trafficking. FEBS Lett. *583*, 3817–3826.

Coco, S., Raposo, G., Martinez, S., Fontaine, J.J., Takamori, S., Zahraoui, A., Jahn, R., Matteoli, M., Louvard, D., and Galli, T. (1999). Subcellular localization of tetanus neurotoxin-insensitive vesicle-associated membrane protein (VAMP)/VAMP7 in neuronal cells: evidence for a novel membrane compartment. J. Neurosci. *19*, 9803–9812.

Colland, F., Jacq, X., Trouplin, V., Mougin, C., Groizeleau, C., Hamburger, A., Meil, A., Wojcik, J., Legrain, P., and Gauthier, J.M. (2004). Functional proteomics mapping of a human signaling pathway. Genome Res. *14*, 1324–1332.

Cotrufo, T., Pérez-Brangulí, F., Muhaisen, A., Ros, O., Andrés, R., Baeriswyl, T., Fuschini, G., Tarrago, T., Pascual, M., Ureña, J., et al. (2011). A signaling mechanism coupling netrin-1/deleted in colorectal cancer chemoattraction to SNARE-mediated exocytosis in axonal growth cones. J. Neurosci. *31*, 14463–14480.

Danglot, L., Triller, A., and Bessis, A. (2003). Association of gephyrin with synaptic and extrasynaptic GABAA receptors varies during development in cultured hippocampal neurons. Mol. Cell. Neurosci. *23*, 264–278.

Danglot, L., Chaineau, M., Dahan, M., Gendron, M.-C., Boggetto, N., Perez, F., and Galli, T. (2010). Role of TI-VAMP and CD82 in EGFR cell-surface dynamics and signaling. J. Cell Sci. *123*, 723–735.

Danglot, L., Zylbersztejn, K., Petkovic, M., Gauberti, M., Meziane, H., Combe, R., Champy, M.F., Birling, M.C., Pavlovic, G., Bizot, J.C., et al. (2012). Absence of TI-VAMP/Vamp7 leads to increased anxiety in mice. J. Neurosci. *32*, 1962–1968.

Desnos, C., Schonn, J.S., Huet, S., Tran, V.S., El-Amraoui, A., Raposo, G.A., Fanget, I., Chapuis, C., Ménasché, G., de Saint Basile, G., et al. (2003). Rab27A and its effector MyRIP link secretory granules to F-actin and control their motion towards release sites. J. Cell Biol. *163*, 559–570.

Echard, A., Jollivet, F., Martinez, O., Lacapère, J.J., Rousselet, A., Janoueix-Lerosey, I., and Goud, B. (1998). Interaction of a Golgi-associated kinesin-like protein with Rab6. Science *279*, 580–585.

Fader, C.M., Sánchez, D.G., Mestre, M.B., and Colombo, M.I. (2009). TI-VAMP/VAMP7 and VAMP3/cellubrevin: two v-SNARE proteins involved in specific steps of the autophagy/multivesicular body pathways. Biochim. Biophys. Acta *1793*, 1901–1916.

Formstecher, E., Aresta, S., Collura, V., Hamburger, A., Meil, A., Trehin, A., Reverdy, C., Betin, V., Maire, S., Brun, C., et al. (2005). Protein interaction mapping: a Drosophila case study. Genome Res. *15*, 376–384.

Fromont-Racine, M., Rain, J.C., and Legrain, P. (1997). Toward a functional analysis of the yeast genome through exhaustive two-hybrid screens. Nat. Genet. *16*, 277–282.

Fukuda, M., and Kuroda, T.S. (2002). Slac2-c (synaptotagmin-like protein homologue lacking C2 domains-c), a novel linker protein that interacts with Rab27, myosin Va/VIIa, and actin. J. Biol. Chem. *277*, 43096–43103.

Goud, B., and Gleeson, P.A. (2010). TGN golgins, Rabs and cytoskeleton: regulating the Golgi trafficking highways. Trends Cell Biol. *20*, 329–336.

Grigoriev, I., Splinter, D., Keijzer, N., Wulf, P.S., Demmers, J., Ohtsuka, T., Modesti, M., Maly, I.V., Grosveld, F., Hoogenraad, C.C., and Akhmanova, A. (2007). Rab6 regulates transport and targeting of exocytotic carriers. Dev. Cell *13*, 305–314.

Grigoriev, I., Yu, K.L., Martinez-Sanchez, E., Serra-Marques, A., Smal, I., Meijering, E., Demmers, J., Peränen, J., Pasterkamp, R.J., van der Sluijs, P., et al. (2011). Rab6, Rab8, and MICAL3 cooperate in controlling docking and fusion of exocytotic carriers. Curr. Biol. *21*, 967–974.

Grosshans, B.L., Ortiz, D., and Novick, P. (2006). Rabs and their effectors: achieving specificity in membrane traffic. Proc. Natl. Acad. Sci. USA *103*, 11821–11827.

Gupton, S.L., and Gertler, F.B. (2010). Integrin signaling switches the cytoskeletal and exocytic machinery that drives neuritogenesis. Dev. Cell *18*, 725–736.

Hebert, B., Costantino, S., and Wiseman, P.W. (2005). Spatiotemporal image correlation spectroscopy (STICS) theory, verification, and application to protein velocity mapping in living CHO cells. Biophys. J. *88*, 3601–3614.

Hill, D.B., Plaza, M.J., Bonin, K., and Holzwarth, G. (2004). Fast vesicle transport in PC12 neurites: velocities and forces. Eur. Biophys. J. *33*, 623–632.

Hoogenraad, C.C., and Bradke, F. (2009). Control of neuronal polarity and plasticity—a renaissance for microtubules? Trends Cell Biol. *19*, 669–676.

Hua, Z., Leal-Ortiz, S., Foss, S.M., Waites, C.L., Garner, C.C., Voglmaier, S.M., and Edwards, R.H. (2011). v-SNARE composition distinguishes synaptic vesicle pools. Neuron *71*, 474–487.

Kakinuma, T., Ichikawa, H., Tsukada, Y., Nakamura, T., and Toh, B.H. (2004). Interaction between p230 and MACF1 is associated with transport of a glycosyl phosphatidyl inositol-anchored protein from the Golgi to the cell periphery. Exp. Cell Res. *298*, 388–398.

Kloepper, T.H., Kienle, C.N., and Fasshauer, D. (2008). SNAREing the basis of multicellularity: consequences of protein family expansion during evolution. Mol. Biol. Evol. *25*, 2055–2068.

Kodama, A., Karakesisoglou, I., Wong, E., Vaezi, A., and Fuchs, E. (2003). ACF7: an essential integrator of microtubule dynamics. Cell *115*, 343–354.

Konishi, Y., and Setou, M. (2009). Tubulin tyrosination navigates the kinesin-1 motor domain to axons. Nat. Neurosci. *12*, 559–567.

Li, F., Pincet, F., Perez, E., Eng, W.S., Melia, T.J., Rothman, J.E., and Tareste, D. (2007). Energetics and dynamics of SNAREpin folding across lipid bilayers. Nat. Struct. Mol. Biol. *14*, 890–896.

Lin, C.M., Chen, H.J., Leung, C.L., Parry, D.A., and Liem, R.K. (2005). Microtubule actin crosslinking factor 1b: a novel plakin that localizes to the Golgi complex. J. Cell Sci. *118*, 3727–3738.

Lochner, J.E., Kingma, M., Kuhn, S., Meliza, C.D., Cutler, B., and Scalettar, B.A. (1998). Real-time imaging of the axonal transport of granules containing a tissue plasminogen activator/green fluorescent protein hybrid. Mol. Biol. Cell *9*, 2463–2476.

Martinez-Arca, S., Alberts, P., Zahraoui, A., Louvard, D., and Galli, T. (2000). Role of tetanus neurotoxin insensitive vesicle-associated membrane protein (TI-VAMP) in vesicular transport mediating neurite outgrowth. J. Cell Biol. *149*, 889–900.

Martinez-Arca, S., Rudge, R., Vacca, M., Raposo, G., Camonis, J., Proux-Gillardeaux, V., Daviet, L., Formstecher, E., Hamburger, A., Filippini, F., et al. (2003). A dual mechanism controlling the localization and function of exocytic v-SNAREs. Proc. Natl. Acad. Sci. USA *100*, 9011–9016.

Matsuzaki, F., Shirane, M., Matsumoto, M., and Nakayama, K.I. (2011). Protrudin serves as an adaptor molecule that connects KIF5 and its cargoes in vesicular transport during process formation. Mol. Biol. Cell *22*, 4602–4620.

Miserey-Lenkei, S., Chalancon, G., Bardin, S., Formstecher, E., Goud, B., and Echard, A. (2010). Rab and actomyosin-dependent fission of transport vesicles at the Golgi complex. Nat. Cell Biol. *12*, 645–654.

Moreau, K., Ravikumar, B., Renna, M., Puri, C., and Rubinsztein, D.C. (2011). Autophagosome precursor maturation requires homotypic fusion. Cell *146*, 303–317.

Pfeffer, S.R. (2007). Unsolved mysteries in membrane traffic. Annu. Rev. Biochem. *76*, 629–645.

Pfenninger, K.H. (2009). Plasma membrane expansion: a neuron's Herculean task. Nat. Rev. Neurosci. *10*, 251–261.

Proux-Gillardeaux, V., Raposo, G., Irinopoulou, T., and Galli, T. (2007). Expression of the Longin domain of TI-VAMP impairs lysosomal secretion and epithelial cell migration. Biol. Cell *99*, 261–271.

Pryor, P.R., Mullock, B.M., Bright, N.A., Lindsay, M.R., Gray, S.R., Richardson, S.C., Stewart, A., James, D.E., Piper, R.C., and Luzio, J.P. (2004). Combinatorial SNARE complexes with VAMP7 or VAMP8 define different late endocytic fusion events. EMBO Rep. *5*, 590–595.

Pryor, P.R., Jackson, L., Gray, S.R., Edeling, M.A., Thompson, A., Sanderson, C.M., Evans, P.R., Owen, D.J., and Luzio, J.P. (2008). Molecular basis for the sorting of the SNARE VAMP7 into endocytic clathrin-coated vesicles by the ArfGAP Hrb. Cell *134*, 817–827.

Reed, N.A., Cai, D., Blasius, T.L., Jih, G.T., Meyhofer, E., Gaertig, J., and Verhey, K.J. (2006). Microtubule acetylation promotes kinesin-1 binding and transport. Curr. Biol. *16*, 2166–2172.

Rink, J., Ghigo, E., Kalaidzidis, Y., and Zerial, M. (2005). Rab conversion as a mechanism of progression from early to late endosomes. Cell *122*, 735–749.

Sankaranarayanan, S., De Angelis, D., Rothman, J.E., and Ryan, T.A. (2000). The use of pHluorins for optical measurements of presynaptic activity. Biophys. J. *79*, 2199–2208.

Scheuber, A., Rudge, R., Danglot, L., Raposo, G., Binz, T., Poncer, J.C., and Galli, T. (2006). Loss of AP-3 function affects spontaneous and evoked release at hippocampal mossy fiber synapses. Proc. Natl. Acad. Sci. USA *103*, 16562–16567.

Simpson, J.C., Griffiths, G., Wessling-Resnick, M., Fransen, J.A., Bennett, H., and Jones, A.T. (2004). A role for the small GTPase Rab21 in the early endocytic pathway. J. Cell Sci. *117*, 6297–6311.

Stenmark, H. (2009). Rab GTPases as coordinators of vesicle traffic. Nat. Rev. Mol. Cell Biol. *10*, 513–525.

Sun, D., Leung, C.L., and Liem, R.K. (2001). Characterization of the microtubule binding domain of microtubule actin crosslinking factor (MACF): identification of a novel group of microtubule associated proteins. J. Cell Sci. *114*, 161–172.

Tamura, K., Ohbayashi, N., Ishibashi, K., and Fukuda, M. (2011). Structure-function analysis of VPS9-ankyrin-repeat protein (Varp) in the trafficking of tyrosinase-related protein 1 in melanocytes. J. Biol. Chem. *286*, 7507–7521.

Tojima, T., Akiyama, H., Itofusa, R., Li, Y., Katayama, H., Miyawaki, A., and Kamiguchi, H. (2007). Attractive axon guidance involves asymmetric membrane transport and exocytosis in the growth cone. Nat. Neurosci. *10*, 58–66.

Verhey, K.J., Kaul, N., and Soppina, V. (2011). Kinesin assembly and movement in cells. Annu. Rev. Biophys. *40*, 267–288.

Wiseman, P.W., Brown, C.M., Webb, D.J., Hebert, B., Johnson, N.L., Squier, J.A., Ellisman, M.H., and Horwitz, A.F. (2004). Spatial mapping of integrin interactions and dynamics during cell migration by image correlation microscopy. J. Cell Sci. *117*, 5521–5534.

Xu, M., Gu, Y., Barry, J., and Gu, C. (2010). Kinesin I transports tetramerized Kv3 channels through the axon initial segment via direct binding. J. Neurosci. *30*, 15987–16001.

Yoshino, A., Setty, S.R., Poynton, C., Whiteman, E.L., Saint-Pol, A., Burd, C.G., Johannes, L., Holzbaur, E.L., Koval, M., McCaffery, J.M., and Marks, M.S. (2005). tGolgin-1 (p230, golgin-245) modulates Shiga-toxin transport to the Golgi and Golgi motility towards the microtubule-organizing centre. J. Cell Sci. *118*, 2279–2293.

Zerial, M., and McBride, H. (2001). Rab proteins as membrane organizers. Nat. Rev. Mol. Cell Biol. *2*, 107–117.

Zhang, X., He, X., Fu, X.Y., and Chang, Z. (2006). Varp is a Rab21 guanine nucleotide exchange factor and regulates endosome dynamics. J. Cell Sci. *119*, 1053–1062.